HHS Public Access

Author manuscript

Immunity. Author manuscript; available in PMC 2017 October 18.

Published in final edited form as:

Immunity. 2016 October 18; 45(4): 861–876. doi:10.1016/j.immuni.2016.09.014.

Macrophage Epithelial Reprogramming Underlies Mycobacterial Granuloma Formation and Promotes Infection

Mark R. Cronan[1], **Rebecca W. Beerman**[1], **Allison F. Rosenberg**[1], **Joseph W. Saelens**[1], **Matthew G. Johnson**[2], **Stefan H. Oehlers**[1], **Dana M. Sisk**[1], **Kristen L. Jurcic Smith**[1,3], **Neil A. Medvitz**[4], **Sara E. Miller**[4], **Le A. Trinh**[6], **Scott E. Fraser**[6], **John F. Madden**[4], **Joanne Turner**[7,8], **Jason E. Stout**[2,3], **Sunhee Lee**[1,3], and **David M. Tobin**[1,5,9,*]

[1]Department of Molecular Genetics and Microbiologym, Duke University School of Medicine, Durham, NC 27710, USA

[2]Division of Infectious Diseases, Duke University School of Medicine, Durham, NC 27710, USA

[3]Department of Medicine, Duke University School of Medicine, Durham, NC 27710, USA

[4]Department of Pathology, Duke University School of Medicine, Durham, NC 27710, USA

[5]Department of Immunology, Duke University School of Medicine, Durham, NC 27710, USA

[6]Molecular and Computational Biology and Translational Imaging Center, University of Southern California, Los Angeles, CA 90089, USA

[7]Department of Microbial Infection and Immunity, The Ohio State University, Columbus, OH 43210

[8]Center for Microbial Interface Biology, The Ohio State University, Columbus, OH 43210

SUMMARY

Mycobacterium tuberculosis infection in humans triggers formation of granulomas, tightly organized immune cell aggregates that are the central structure of tuberculosis. Infected and uninfected macrophages interdigitate, assuming an altered, flattened appearance. Although pathologists have described these changes for over a century, the molecular and cellular programs underlying this transition are unclear. Here, using the zebrafish-*Mycobacterium marinum* model, we found that mycobacterial granuloma formation is accompanied by macrophage induction of canonical epithelial molecules and structures. We identified fundamental macrophage

*Correspondence: david.tobin@duke.edu.

9Lead contact

AUTHOR CONTRIBUTIONS

M.R.C. and D.M.T. conceived and designed the project. M.R.C, R.W.B., A.F.R., S.H.O, D.M.S, K.L.J.S., and N.A.M performed and analyzed experiments, J.W.S. performed bioinformatic analyses, M.G.J., J.F.M., and J.E.S. identified and prepared clinical specimens, S.E.M. supervised and analyzed the electron microscopy experiments, L.A.T. and S.E.F. conceived and generated the gene trap lines, J.T. and S.L. designed, performed, and supervised the mouse experiments, M.R.C. and D.M.T. wrote the manuscript with input from all authors.

The accession number for the data reported in this paper is GEO: GSE81913.

reprogramming events that parallel E-cadherin-dependent mesenchymal-epithelial transitions. Macrophage-specific disruption of E-cadherin function resulted in disordered granuloma formation, enhanced immune cell access, decreased bacterial burden and increased host survival, suggesting that the granuloma can also serve a bacteria-protective role. Granuloma macrophages in humans with tuberculosis were similarly transformed. Thus, during mycobacterial infection, granuloma macrophages are broadly reprogrammed by epithelial modules, and this reprogramming alters the trajectory of infection and the associated immune response.

Graphical Abstract

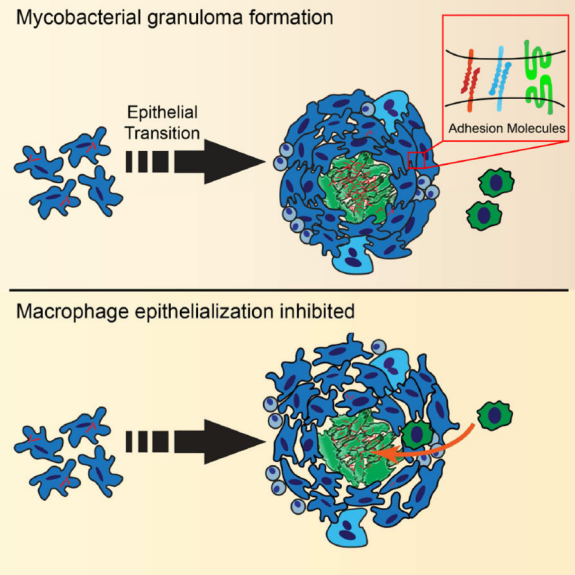

INTRODUCTION

Mycobacterium tuberculosis (*Mtb*), the causative agent of tuberculosis (TB), can reside in a host-derived immune structure termed the granuloma (Ernst, 2012; Martin et al., 2015; Ramakrishnan, 2012). The granuloma is the defining pathological feature of TB, and the name tuberculosis derives from descriptions of granulomas as “tubercles” by early pathologists (Russell, 2007). Although granulomas have traditionally been viewed as a host-protective walling-off of pathogens or antigens resistant to elimination, pathogenic mycobacteria also appear able to accelerate and exploit this host response, promoting disease progression (Martin et al., 2015; Ramakrishnan, 2012; Volkman et al., 2004; Volkman et al., 2010).

Granulomas are macrophage-derived structures, which later recruit other immune cells, and can form in response to a variety of persistent inflammatory or noninflammatory stimuli, including foreign bodies, schistosome eggs, and pathogenic mycobacteria among others (Adams, 1976; Dannenberg, 1968; Williams and Williams, 1983). In schistosomiasis and TB, aggregating macrophages undergo a series of stereotyped morphological changes; their cytoplasm expands, and zipper-like interdigitations form between the apposed membranes of neighboring cells (Adams, 1974, 1976; Dannenberg, 1968; Williams and Williams, 1983).

Histological characterization of this transformation led pathologists to term these macrophages “epithelioid” as far back as at least 1888, due to their abundant cytoplasm, pale, oval nuclei, and close interdigitation with neighboring cells (Adams, 1974, 1976; Metchnikoff, 1888). Although they resemble epithelial cells by histology, the epithelioid cells that form the central scaffold of tuberculous granulomas are thought to be macrophage derived (Adams, 1974; Spector and Lykke, 1966; Spector and Willoughby, 1968; Sutton and Weiss, 1966; Yona and Gordon, 2015).

There is relatively little understanding of the molecular architecture of epithelioid macrophages in TB, a particularly common and important cause of granulomas in humans. Epithelioid cells in other granuloma types can express at least one canonical epithelial marker. In human specimens of sarcoidosis and foreign body granulomas, E-cadherin is expressed in skin granuloma macrophages (Wanat et al., 2014). In cell culture, IL-4/IL-13-treated macrophages have also been shown to express E-cadherin, a finding confirmed in sorted macrophages from mouse helminth infections (Van den Bossche et al., 2009; Van den Bossche et al., 2015).

However, the nature, extent, and consequences of epithelioid transformation in tuberculous granulomas remain largely undefined. The zebrafish-*Mycobacterium marinum* model has emerged as a useful tool for understanding granuloma formation in an optically accessible vertebrate (Ramakrishnan, 2012) and recapitulates key features of human tuberculous granulomas (Davis et al., 2002; Swaim et al., 2006).

Here we used the zebrafish-*M. marinum* model to define key cellular and molecular events that underlie macrophage transformation and granuloma assembly. We found that infected macrophages nucleated specialized networks of macrophage-macrophage adherens junctions that scaffold mycobacterial granulomas. Macrophage-specific disruption of cadherin-mediated adhesion led to disorganized granulomas. This loss of organization resulted in increased immune cell access, decreased bacterial burden, and increased host survival during mycobacterial infection, consistent with bacterial exploitation of the host granuloma niche. Finally, we demonstrated that broad macrophage epithelial reprogramming, analogous to mesenchymal-epithelial transitions, is a conserved feature of mycobacterial granulomas in mouse models and in humans.

RESULTS

Induction of E-cadherin in Macrophages During Granuloma Formation

M. marinum infection of optically transparent zebrafish larvae enables direct visualization of granuloma formation in a natural host. We used this model to assess the nature of macrophage epithelioid transformation during granuloma assembly (Figure 1A). We first asked whether granuloma macrophages deploy true epithelial markers.

Epithelial cells are classically defined by homotypic E-cadherin-positive adherens junctions (Bryant and Mostov, 2008; De Craene and Berx, 2013; van Roy and Berx, 2008). We examined granuloma macrophages for E-cadherin expression. We found robust E-cadherin induction in the granuloma in both infected and uninfected granuloma macrophages (Figure

1B). To confirm E-cadherin expression within macrophages, we co-stained using antibodies specific to the zebrafish leukocyte marker l-plastin (Herbomel et al., 1999). Indeed, these cells were positive for both l-plastin and E-cadherin (Figure 1B). Infected and uninfected macrophages not in granulomas invariably did not express E-cadherin (Figure S1A). Thus granuloma macrophages access a central component of a classical epithelialization program.

Live Imaging of Macrophage Adherens Junction Formation within Granulomas

In epithelial cells, cell-cell adhesions driven by E-cadherin result in the formation of adherens junctions between cells (van Roy and Berx, 2008). To directly investigate the dynamics of adherens junctions during granuloma formation, we identified zebrafish gene trap lines in which animals express fully functional, fluorescently tagged versions of α-catenin (*Gt(ctnna-citrine)*^{ct3a}) or plakoglobin (*Gt(jup-citrine)*^{ct520a}), both members of the adherens junction complex (Figure 1C) (Trinh et al., 2011). Animals homozygous for the gene traps were fully viable, and both gene trap lines showed the expected expression patterns, localizing to the cell membrane of adherens junctions within epithelial tissues (Figure S1B).

Intravital imaging of *M. marinum*-infected animals revealed induction and relocalization of tagged plakoglobin and α-catenin to sites of cell-cell contact within the granuloma by 3 days post-infection (dpi) (Figures 1D–F and S1C–E). At 3 dpi, concurrent with the initial appearance of early granulomas, 30–40% of the total granulomas had membrane-localized expression of the adherens junction component (plakoglobin −60/179 granulomas positive, 23 total animals; α-catenin - 82/198 granulomas positive, 24 total animals). Thus, even at early timepoints, E-cadherin induction is accompanied by formation of adherens junctions within the granuloma.

We confirmed adherens junction formation between macrophages by staining infected plakoglobin gene-trap zebrafish larvae with a pan-keratin antibody to visualize epithelium, and with the anti-l-plastin antibody to visualize leukocytes. In granulomas, we found that the keratin-positive skin epithelium was only present on the exterior, whereas the adherens junctions within were formed between l-plastin-positive leukocytes (Figure S1F). E-cadherin staining of granulomas in α-catenin and plakoglobin gene-trap animals demonstrated that E-cadherin colocalized extensively at cell junctions with both α-catenin and plakoglobin (Figures 1G and 1H).

To capture initial events of granuloma formation, we generated a strain with a macrophage-specific reporter and the plakoglobin gene trap (*Tg(mfap4:tomato-caax); Gt(jup-citrine)*^{ct520a}) and performed long-term imaging of nascent granulomas in infected animals starting at 2 dpi. We captured nucleation of adherens junctions within clusters of granuloma macrophages, often adjacent to epithelium (Figures 2A-2G, arrows and Movie S1). Consistent with our earlier analysis, we found that 25 of 61 granulomas observed during this imaging were plakoglobin positive over this early time-frame.

The initial adherens junctions spread to macrophages deeper within the granuloma (Figures 2E-2J). The propagation of these adherens junctions occurred through interactions of

incoming plakoglobin-negative macrophages with established plakoglobin-positive macrophages (Figure 2I and 2J).

We directly tracked individual cells surrounding the epithelial-macrophage interface and found little evidence for invagination of skin epithelial cells, confirming that formation of adherens junctions involved granuloma macrophages (Movie S2). Images of single planes confirmed that the plakoglobin-expressing cells were positive for the *mfap4* macrophage marker (Figure 2H). Thus, as macrophages form mycobacterial granulomas, they express and deploy adherens junction components.

Adult Mycobacterial Granulomas Form Organized Networks of Epithelial-like Adhesions

M. marinum infection of adult zebrafish can lead to longer-term infections than in larvae (Parikka et al., 2012; Swaim et al., 2006). These granulomas morphologically resemble human granulomas and include additional cell types, including adaptive immune components (Parikka et al., 2012; Swaim et al., 2006; Ulrichs et al., 2004).

In adults at 2 weeks post infection (wpi), we found that plakoglobin-positive adherens junctions were induced within granulomas and colocalized with E-cadherin (Figure 3A). In necrotic granulomas, the adherens junctions consistently formed in concentric layers surrounding the necrotic core (Figure 3A). Hematoxylin and eosin (H&E) staining confirmed that the cells had the characteristic morphology and staining pattern of epithelioid cells (Figure S2A) (Adams, 1974; Swaim et al., 2006).

As in larvae, the plakoglobin-positive cells retained leukocyte markers, including l-plastin (Figure 3B). We also stained for the epithelial markers p63 and pan-keratin. Neither marker stained cells within the granuloma (Figures S2C and S2D), but we observed staining in epithelial tissues including skin (stained by both p63 and keratin), intestine (keratin) and pancreas (keratin) (Figure S2B and S2D). These results suggest that the E-cadherin-positive cells of the granuloma are hematopoietic in origin and not a population of infiltrating epithelial cells.

Lineage Tracing Identifies Macrophage-Macrophage Adherens Junctions

We used macrophage-specific lineage tracing to assess the origin of the E-cadherin-positive cells more definitively. We found that the established macrophage markers, *mpeg1* and *mfap4* (Ellett et al., 2011; Walton et al., 2015; Zakrzewska et al., 2010) were repressed in adult granulomas, although the *mfap4* reporter could still be detected in larval granulomas (Figures 2, and S2E-S2F). This result suggested either a different origin of epithelioid cells in adults or a more fundamental macrophage reprogramming associated with granuloma formation.

We therefore developed a lineage-tracing approach in which a previously characterized macrophage-specific Cre line, *Tg(mfap4:icre-p2a-tomato)*^{xt8} (denoted *mfap4:icre* hereafter) (Figure 3C) (Walton et al., 2015), drove rearrangement of a floxed reporter line, *Tg(ubb:loxp-tagbfp2-stop-loxp-tomato)*^{xt7} (denoted *ubb:BSR* for Blue-Stop-Red hereafter). The Cre-positive macrophages in the absence of the floxed transgene displayed only weak expression of tdTomato (Figure 3D). Cre-induced recombination of the indicator line

resulted in bright macrophage tdTomato fluorescence driven off of the *ubb* promoter (Mosimann et al., 2011), easily distinguishable from macrophages expressing Cre only (Figure 3D).

We infected *Tg(mfap4:icre; ubb:BSR); Gt(jup-citrine)*^{ct520a} animals with *M. marinum* and examined granulomas at 2 wpi. As predicted, many of the plakoglobin-positive cells surrounding the necrotic core were from the macrophage lineage (Figure 3E). We also found that macrophages within non-necrotic granulomas formed plakoglobin-positive adherens junctions (Figure S3A). Not every macrophage was labeled by the lineage-tracing approach (presumably a limitation of promoter strength and Cre efficacy), but we consistently identified macrophage-macrophage adherens junctions in both necrotic and non-necrotic adult granulomas (Figures 3E and S3A, arrows). Infected and uninfected macrophages outside the granuloma failed to express plakoglobin (Figure S3B). These findings further confirmed that granuloma adherens junctions are macrophage derived, suggesting that macrophages undergo a process of epithelialization.

Mycobacterial Granuloma Macrophages Form Classical Epithelial Adherence Structures

We used electron microscopy to investigate the repertoire of adhesive structures within the granuloma. In addition to adherens junctions, we identified both classical desmosomes and tight junctions between granuloma macrophages (Figures 3F and 3G). Desmosomes were accompanied by networks of intermediate filaments entering these structures (Figure 3G).

To visualize tight junctions throughout the granuloma, we stained for the marker ZO-1. ZO-1 staining identified tight junctions throughout the granuloma, particularly in regions surrounding the necrotic core (Figure 4A). Thus, canonical tight junctions, crucial adhesive structures within the apical domain of epithelial cells, are induced in mycobacterial granulomas, suggesting that granuloma macrophages may deploy elements of a classical apico-basal polarity program.

We next investigated whether granuloma formation was accompanied by epithelial-like actin rearrangement within granuloma macrophages. Adherens junction-positive macrophages within both necrotic and non-necrotic granulomas exhibited a cortical actin distribution, as commonly observed in epithelial cells (Figures 4B and S3C, blue arrows). In adherens junction-negative macrophages within the granuloma and tissue resident macrophages, actin was largely organized into cytoplasmic structures and lay away from sites of cell-cell contact (Figures S3C and S3D). In total, these findings indicate that granuloma macrophages undergo a fundamental transition to an epithelial-like state, including the formation of extensive adherens, desmosomal, and tight junctions, and reorganization of their actin cytoskeleton.

Widespread Transcriptional Reprogramming in Granuloma Macrophages

To assess granuloma macrophage reprogramming more comprehensively, we microdissected necrotic granulomas from *M. marinum* infected animals (Figure 4C) and performed RNA-seq. CLARITY processing followed by E-cadherin staining demonstrated that individual granulomas were isolated cleanly and were not disrupted during dissection (Chung et al., 2013; Cronan et al., 2015; Yang et al., 2014). Isolated granulomas had central necrotic foci

replete with bacteria surrounded by intact layers of E-cadherin-positive cells (Figure 4D), in agreement with findings in tissue sections.

We compared the transcriptional profile of isolated granulomas at 2 wpi to macrophages isolated from the kidney of the same animals. Principal component analysis revealed differential clustering of the granuloma samples and the matched macrophages (Figure S4A), and unsupervised hierarchical clustering of transcript profile resulted in divergent clusters between granuloma and matched macrophage samples (Figure 4E). Annotated pathway data as well as full data are presented in Tables S1 and S2, respectively.

We identified differentially regulated KEGG pathways, which included pathways previously associated with *Mtb* granulomas, including cytokine-cytokine receptor interactions, arachidonic acid metabolism, lysosome, and phagosome pathways (Figure 4F). Corroborating our identification of epithelial-like adhesions, we found multiple adhesion pathways significantly differentially regulated between granulomas and the paired macrophage samples (Figure 4F). We also observed significant enrichment of pathway members involved in actin cytoskeleton regulation (Figure 4F), consistent with the reorganization of actin we observed.

Analysis of RNA-seq data for individual genes identified significant upregulation of genes involved in adherens junctions (e.g. E-cadherin, α-catenin, β-catenin, plakoglobin and δ-catenin), tight junctions (ZO-1, ZO-2, several claudins) and desmosomes (desmoplakin, desmoglein and desmocollin) (Figure 4G, Table S1 and Table S2). As we observed tight junction formation within the granuloma, which generally marks the apical surfaces of cells, we also investigated whether cell polarity markers were induced. We identified significant induction of a number of apical (Par3, Par6, aPKC) and basal (Lgl, Dig) polarity markers, suggesting that granulomas may access cell polarity programs.

We further investigated the polarization of the granuloma by visualizing the basement membrane using fibronectin staining. Punctate fibronectin staining surrounded the granuloma, suggesting that granulomas may form a basement membrane-positive basal region (Figure S4B).

We also examined the expression of a number of macrophage and leukocyte markers within the granuloma (Figure 4G). While most of these markers were lower in the granuloma than in isolated macrophages, we found that macrophage marker expression levels were significantly higher in granulomas than in control cell populations (Table S1), suggesting at least some retention of macrophage identity. In total, these results suggest that macrophages undergo an extensive and specific reprogramming that drives an epithelial-like program and includes multiple components of classical epithelial and cell polarity modules.

Inhibition of Cadherin-Mediated Adhesion Alters Granuloma Morphology

We next assessed the functional contribution of epithelialization to granuloma organization and infection trajectory. E-cadherin serves as a central mediator of epithelialization; loss of E-cadherin in epithelial populations causes them to lose epithelial character and acquire mesenchymal morphology. We generated a dominant negative (DN) zebrafish E-cadherin

construct using a truncated intracellular domain of E-cadherin driven to the membrane by an N-terminal myristoylation signal (Nieman et al., 1999).

To confirm that this construct was functional in zebrafish, we expressed the DN-E-cadherin construct transiently and mosaically in injected zebrafish larvae. Mosaic expression of DN-E-cadherin led to high rates of lethality. In surviving animals (in which DN-E-cadherin was expressed in a narrow population of cells) we observed that the red DN-E-cadherin-expressing cells frequently protruded from surrounding epithelial layers and live red cells were readily extruded from the skin (Figure S4C).

Having validated the construct, we used a lineage-tracing approach to enable selective expression of DN-E-cadherin within specific cell populations. We first generated *Tg(ubb:loxP-gfp-stop-loxP-DN-e-cadherin-p2a-tomato)*^{xt9} (hereafter denoted *ubb:GS-DN-e-cadherin* for Green-Stop-DN-e-cadherin) (Figure 5A). Crossing this line to the *Tg(mfap4:icre)* driver line led to selective rearrangement of the cassette in macrophages and expression of DN-E-cadherin as assessed by tomato fluorescence (Figure 5B).

We infected adult *Tg(mfap4:icre; ubb:GS-DN-e-cadherin)* and control *Tg(mfap4:icre; ubb:BSR)* animals with *M. marinum* and evaluated granuloma formation at 2 wpi. Granulomas in *Tg(mfap4:icre; ubb:GS-DN-e-cadherin)* animals were less organized and devoid of the organized layer of cells that surrounds the necrotic center of control granulomas (Figures 5C, 5E and S4D). H&E staining of control and DN-E-cadherin-expressing animals further confirmed the disorganization of granulomas in these animals (Figures 5D and S5A). Granuloma macrophages in DN-E-cadherin-expressing animals frequently had an elongated, spindle morphology and reduced cytoplasm as opposed to epithelioid morphology and abundant cytoplasm in controls (Figure 5D, arrows). Not only was the morphology of necrotic granulomas altered in *Tg(mfap4:icre; ubb:GS-DN-e-cadherin)* animals, but we also found that the proportion of necrotic granulomas in *Tg(mfap4:icre; ubb:GS-DN-e-cadherin)* animals was elevated (Figure 5F).

We generated an independent lineage tracing DN-E-cadherin construct *Tg(ubb:loxP-tagbfp2-stop-loxP-DN-e-cadherin-p2a-tomato)*^{xt10} (designated *ubb:BS-DN-e-cadherin* for Blue-Stop-DN-e-cadherin from here on) (Figure 5G). Non-rearranged cells express blue fluorescent protein to be compatible with the citrine-expressing α-catenin and plakoglobin gene trap constructs (Figure 5G). Crossing to the *Tg(mfap4:icre)* driver line caused efficient rearrangement of the DN-E-cadherin cassette (Figure 5H). As expected, macrophage-specific DN-E-cadherin expression diminished the formation of plakoglobin-positive adherens junctions in granuloma macrophages relative to control animals (Figures 5I and 5J). Granulomas formed in *Tg(mfap4:icre; ubb:BS-DN-e-cadherin); Gt(jup-citrine)*^{ct520a} animals at 2 wpi demonstrated a similar loss of granuloma organization and increased necrotic granuloma frequency relative to *Tg(mfap4:icre; ubb:BSR); Gt(jup-citrine)*^{ct520a} control animals (Figures 5E and 5F).

To better assess the morphological transformations within the granuloma, we used CLARITY to clear dissected zebrafish organs (Figure 5K) (Chung et al., 2013; Cronan et al., 2015; Yang et al., 2014). In control *(Tg(mfap4:icre; ubb:BSR); Gt(jup-citrine)*^{ct520a}*)*

animals, the bacteria-laden core of the granuloma was surrounded by adherens junctions (Figure 5L, Movie S3). In contrast, DN-E-cadherin expression in macrophages (*Tg(mfap4:icre; ubb:BS-DN-e-cadherin); Gt(jup-citrine)*^{ct520a}*)* resulted in granulomas that were diffuse, with minimal adherens junctions and which, in many cases, failed to organize (Figure 5L, Movie S4). Even the subset of DN-E-cadherin granulomas that were better organized had a thinner layer of adherens junctions around the bacterial core, with intermittent gaps (Figure S5B, arrows, and Movie S5).

Cadherin-disrupted Granulomas Lead to Improved Host Outcome

To investigate the functional outcome of disrupted granuloma formation, we infected adult *Tg(mfap4:icre; ubb:BSR)* and *Tg(mfap4:icre; ubb:GS-DN-e-cadherin)* animals with *M. marinum*, measured bacterial burden and also assessed long term survival. At 2 wpi, bacterial burden was reduced in DN-E-cadherin expressing animals both by CFU assays and quantitation of bacterial fluorescence in matched sections of kidney tissue (Figures 6A and S5C). Consistent with decreased burden, we found that *Tg(mfap4:icre; ubb:GS-DN-e-cadherin)* animals survived longer (median survival of 37 days in control animals vs 83 days in DN-E-cadherin expressing animals) than matched *Tg(mfap4:icre; ubb:BSR)* control animals (Figures 6B and S5D–S5E).

To further investigate the enhanced survival of DN-E-cadherin positive animals, we harvested *Tg(mfap4:icre; ubb:GS-DN-e-cadherin)* animals that had survived to three months post-infection (all of the matched control animals had died by this timepoint). We found that by either bacterial fluorescence or acid-fast staining these animals contained numerous granulomas that were apparently sterile (Figures S5F and S5G). Together, these experiments suggest that granuloma epithelialization can benefit the bacterium.

We examined multiple aspects of macrophage development and function and found no differences prior to granuloma formation. Quantitation in *Tg(mfap4:icre; ubb:GS-DN-e-cadherin)* larval zebrafish demonstrated that DN-E-cadherin expression within macrophages did not lead to alterations in macrophage number (Figures S6A and S6B); changes in phagocytosis (Figures S6C and S6D); intracellular growth (Figure S6E); or bacterial burden at early infection timepoints (Figure S6F). Thus, DN-E-cadherin expression had little effect on macrophage development and function in early infection.

Granuloma Disruption Results in Increased Immune Cell Access

Intact organized granulomas might, in parallel to epithelial barriers, limit immune access or immune recognition of the bacteria contained within, providing a relatively protected niche for bacterial proliferation. We tested a number of T cell antibodies but were unable to find an antibody that performed acceptably on zebrafish tissue sections. We instead tested the accessibility of neutrophils to the interior of the granuloma. By staining for the zebrafish neutrophil marker LysC (Hall et al., 2007; Meijer et al., 2008), we found that neutrophils preferentially reached the interior of granulomas in DN-E-cadherin expressing animals (Figures 6C and 6D).

Because the lineage tracing disruptions were not fully efficient, we could also identify mosaic granulomas in the macrophage-specific DN-E-cadherin animals in which some of

each granuloma contained plakoglobin-positive adherens junctions while other parts were disrupted (Figure 6E). Neutrophil numbers were specifically enriched in the plakoglobin-negative areas of granulomas relative to the plakoglobin-positive areas, suggesting that these adhesions control local immune access or recognition of bacteria (Figures 6E and 6F).

Macrophages in Human Mycobacterial Granulomas Express E-cadherin

To extend our findings from zebrafish to humans, we investigated E-cadherin expression within the macrophages of human granulomas. We obtained clinical samples of granulomas from Mfb-infected patients as well as patients infected with non-tuberculous mycobacteria. Granuloma macrophages stained positive for E-cadherin in each of nine specimens from eight distinct patients (Figures 7A–C and S7A–S7C). In non-necrotic *Mtb* granulomas, E-cadherin localized to cell-cell junctions in groups of macrophages throughout the granuloma, similar to non-necrotic zebrafish granulomas (Figure 7A). Dual staining for the macrophage marker CD68 and E-cadherin demonstrated that the E-cadherin positive cells within human granulomas are macrophages (Figure 7B). In both *Mtb* and *M. avium* necrotic granulomas in lung and lymph node tissue, we found prominent E-cadherin localization within the palisading macrophages directly around the necrotic core, mimicking the layers of E-cadherin positive cells surrounding the necrotic core of zebrafish granulomas (Figure 7C and Figure S4A–S4C).

We also investigated E-cadherin induction during *Mtb* infection of mice. Macrophages in C57BL/6 *Mtb* granulomas expressed E-cadherin (Figure 7D). However, E-cadherin expression generally localized to the cytoplasm of the macrophages and sporadically to the cell membrane. C57BL/6 mice are relatively resistant to *Mtb* infection and form relatively loose granulomas (Medina and North, 1998). To examine macrophage E-cadherin induction in a more susceptible mouse strain, we performed E-cadherin staining of *Mtb* granulomas in CBA/J mice (Beamer et al., 2008; Turner et al., 2001). Although CBA/J granulomas are also relatively disorganized, we found that E-cadherin was again induced in granuloma macrophages, and that E-cadherin in this case was more consistently membrane localized (Figure 7E). Thus, macrophage induction of E-cadherin-positive junctions during mycobacterial granuloma formation is conserved in zebrafish, mice, and humans.

DISCUSSION

Here we describe the molecular underpinnings of macrophage epithelialization in the tuberculous granuloma. The histopathological features of TB were first described in the 19th century (Adams, 1976; Schüppel, 1871). The defining characteristic of the granuloma has long been the aggregation of a distinct subtype of macrophages, termed epithelioid, which interdigitate and take on a flattened appearance, with expanded cytoplasm and ovoid nuclei (Adams, 1974). Despite extensive characterization of the granuloma and the cells within, the cellular and molecular nature of this key phenotypic transformation remains largely unknown. We found that, in mycobacterial infections, macrophages formed macrophage-macrophage adherens junctions, desmosomes, and tight junctions during granuloma formation and that this process drives the trajectory of disease.

We identified broad epithelial modules engaged by granuloma macrophages. These cells showed reduced expression of macrophage markers, consistent with the extensive transformations within these macrophage populations, but still expressed macrophage and leukocyte markers above background. While there is strong induction of epithelial modules and structures, the transition may not be total. We did not see granuloma macrophage staining using a pan-keratin antibody (although several keratins were enriched by RNA-seq).

We found macrophage epithelialization to be conserved in human mycobacterial granulomas. Recently, profiling of a small number of human granulomas generated a proteomic dataset (Marakalala et al., 2016). We examined these data and, in agreement with the zebrafish data, identified induction of desmosomal proteins (desmoplakin, desmoglein and desmocollin), adherens junction proteins (E-cadherin, plakoglobin, α-, β-, δ- catenin) and tight junction pathways (ZO-1 and ZO-2) within the epithelioid macrophage layer of human granulomas (Marakalala et al., 2016). A previous report has also identified desmosome formation within granulomas from striped bass through electron microscopy (Gauthier et al., 2004).

There is some precedent for induction of at least E-cadherin in other granuloma types. One report has described E-cadherin expression in cutaneous granulomas in foreign body reactions and sarcoidosis (Wanat et al., 2014), while expression of E-cadherin in sorted macrophages from mouse helminth infections suggests induction of E-cadherin in another granulomatous disease (Van den Bossche et al., 2015).

In schistosome granulomas, macrophage-specific deletion of E-cadherin did not alter granuloma architecture (Van den Bossche et al., 2015). It is possible that mechanisms differ between helminth-induced and mycobacterial granulomas. However, it has also been reported that elicited macrophages in mouse models of schistosomiasis can resist LysM:Cre-mediated deletion (Vannella et al., 2014), and so definitive comparison of the functional role of E-cadherin in distinct granuloma types may require further analysis.

Notably, Langerhans cells also express E-cadherin as they interact with keratinocytes (Tang et al., 1993). This differs from our findings, as we do not observe baseline expression of E-cadherin within macrophages, nor is there evidence for homotypic Langerhans cell interactions.

Our results with macrophage reprogramming and granuloma formation suggest a parallel to developmental transformations. Expression of E-cadherin within motile mesenchymal populations can transition the cells into epithelial morphology in a process called mesenchymal-epithelial transition (MET) (Bryant and Mostov, 2008; De Craene and Berx, 2013). These morphological programs have been described in development and cancer, where they are critical mediators of gene expression and cell behavior (Bryant and Mostov, 2008; De Craene and Berx, 2013), but immune cell populations have generally not been considered a part of this framework.

In mosaic DN-E-cadherin granulomas, there was increased neutrophil recruitment to granuloma regions lacking adherens junctions. Decreased bacterial burden may be due in part to increased immune access to the interior. Neutrophils have been associated with both

improved and worsened host outcomes in TB (Dallenga and Schaible, 2016; Yang et al., 2012). It is possible that some of the host-detrimental effects of neutrophil interactions may be mediated by their recruitment and nonproductive activation in areas in which there is an epithelial-like barrier between them and the infecting bacteria. Increased immune cell accessibility in disrupted granulomas is likely to apply to other immune cell types known to play important roles in protection.

Overall, these findings lend mechanistic support to the idea that a classically organized granuloma can be a favorable niche for mycobacteria (Dorhoi and Kaufmann, 2014; Philips and Ernst, 2012; Ramakrishnan, 2012; Volkman et al., 2004). The increased survival in animals with disrupted granuloma adherens junctions points to the possibility of modulating granuloma stability to enhance existing therapies. More generally, these results suggest that immune cells engage canonical developmental and epithelial programs to construct a central structure of tuberculosis.

EXPERIMENTAL PROCEDURES

Zebrafish Handling and Strains

Zebrafish experiments were performed with the approval of the Duke University Animal Care and Use Committee (protocol A145-14-06). Larvae were raised in filtered fish system water. For imaging, pigmentation was halted through addition of 45 μg/ml 1-phenyl-2-thiourea (PTU) at one dpf. *Tg(mpeg1:tomato-caax)*^{xt3}, *Tg(mfap4:icre-p2a-tomato)*^{xt8}, *Tg(mfap4:tomato-caax)*^{xt6} and *Gt(ctnna-citrine)*^{ct3a} lines have been previously described (Oehlers et al., 2015; Trinh et al., 2011; Walton et al., 2015).

Larval and Adult Zebrafish Infections and Bacterial Burden determination

Larval and adult zebrafish were anesthetized with tricaine (MS-222, final concentration 0.016%). For larvae, approximately 200 fluorescent bacteria (FB) of *M. marinum* were injected into the caudal vein of each embryo. For adults, either 400 FB or 50 FB were injected intraperitoneally.

Larval bacterial burdens were determined by quantitating bacterial fluorescence by microscopy. Adult bacterial burden was determined by CFU assay.

Statistics

Statistical analyses utilized for each data set are indicated in figure legends. All statistical analyses were performed using Prism 5 (GraphPad Software).

Staining of Larval Zebrafish and Frozen Sectioning and Immunostaining of Adult Zebrafish

4 dpi larvae were fixed in Dent's Fixative (80% methanol, 20% DMSO), blocked in 3% goat serum and stained with primary and secondary antibodies.

For neutral red staining, 3dpf larvae were soaked in Neutral Red (Sigma N6264) 2.5μg/ml overnight at 28.5C.

2 wpi adult zebrafish were euthanized, fixed in 4% PFA and frozen in Neg-50 (Richard Allen Scientific). Zebrafish were cryosectioned at 20 μm.

For immunostaining, sections from adult fish, were blocked in 3% goat serum and stained with primary and secondary antibodies as indicated.

Human Patient Samples

Human research was approved by the Duke Medicine Institutional Review Board under protocol number Pro00057484. Human tissue samples containing mycobacterial granulomas were identified. Tissue specimens were obtained from the pathology department, and paraffin sections cut by the Duke Pathology Research Histology Laboratory.

Staining of Human and Mouse Tissues

Sections were deparaffinized and rehydrated. Sections underwent antigen retrieval followed by blocking. For immunohistochemistry, sections were incubated with primary and HRP conjugated secondary antibodies. Sections were developed with ImmPACT DAB (Vector Laboratories). For immunofluorescence, sections were incubated with primary antibodies followed by Alexafluor conjugated secondary antibodies (Thermo-Fisher).

Additional Experimental Procedures

Detailed experimental methods about generation of transgenic zebrafish lines, bacterial strains, generation of transgene constructs, larval and adult zebrafish infections, bacterial burden determination in infected adults, microscopy and image quantitation, electron microscopy, staining of larval zebrafish, neutral red staining, quantitation of phagocytic macrophages in larvae, quantitation of bacteria per macrophage, quantifying larval mycobacterial burden, sectioning and histology of adult zebrafish, identification and quantitation of granulomas, RNA-Seq of adult zebrafish granulomas, CLARITY clearing of dissected organs and granulomas, human patient samples, mouse-Mfb infections and sectioning, and immunostaining of human and mouse tissues are available in Supplemental Experimental Procedures.

Supplementary Material

Refer to Web version on PubMed Central for supplementary material.

Acknowledgments

We thank Yi Feng for l-plastin antibodies, S. Abraham, J. Coers, M. Matty, and L. Ramakrishnan for helpful discussions and comments, A. Sagasti for suggesting the gene trap lines, and W. Terrell for assistance with clinical samples. This work was funded by an American Cancer Society Postdoctoral Fellowship PF-13-223-01-MPC (M.R.C.); an NIH Training Grant for Immunological Diseases 5T32AI007217-33 (A.F.R); an Australian NHMRC Early Career Fellowship (S.H.O.); an NSF Graduate Fellowship (J.W.S.); a Duke University NIH AIDS Training Grant (5T32AI007392) (M.G.J.); the Duke Center for AIDS Research, an NIH funded program (5P30 AI064518), and a Searle Scholar Award, a Vallee Foundation Young Investigator Award, and an NIH Director's New Innovator Award 1DP2-OD008614 (D.M.T.).

REFERENCES

Adams DO. The structure of mononuclear phagocytes differentiating in vivo. I. Sequential fine and histologic studies of the effect of Bacillus Calmette-Guerin (BCG). Am JPathol. 1974; 76:17–48. [PubMed: 4601921]

Adams DO. The granulomatous inflammatory response. A review. Am J Pathol. 1976; 84:164–192. [PubMed: 937513]

Beamer GL, Flaherty DK, Assogba BD, Stromberg P, Gonzalez-Juarrero M, de Waal Malefyt R, Vesosky B, Turner J. lnterleukin-10 promotes Mycobacterium tuberculosis disease progression in CBA/J mice. J Immunol. 2008; 181:5545–5550. [PubMed: 18832712]

Bryant DM, Mostov KE. From cells to organs: building polarized tissue. Nat Rev Mol Cell Biol. 2008; 9:887–901. [PubMed: 18946477]

Chung K, Wallace J, Kim SY, Kalyanasundaram S, Andalman AS, Davidson TJ, Mirzabekov JJ, Zalocusky KA, Mattis J, Denisin AK, et al. Structural and molecular interrogation of intact biological systems. Nature. 2013; 497:332–337. [PubMed: 23575631]

Cronan MR, Rosenberg AF, Oehlers SH, Saelens JW, Sisk DM, Smith KL, Lee S, Tobin DM. CLARITY and PACT-based imaging of adult zebrafish and mouse for whole-animal analysis of infections. Dis Model Mech. 2015; 8:1643–1650. [PubMed: 26449262]

Dallenga T, Schaible UE. Neutrophils in tuberculosis-first line of defence or booster of disease and targets for host-directed therapy? Pathog Dis. 2016; 74

Dannenberg AM Jr. Cellular hypersensitivity and cellular immunity in the pathogensis of tuberculosis: specificity, systemic and local nature, and associated macrophage enzymes. Bacteriol Rev. 1968; 32:85–102. [PubMed: 4873814]

Davis JM, Clay H, Lewis JL, Ghori N, Herbomel P, Ramakrishnan L. Real-time visualization of mycobacterium-macrophage interactions leading to initiation of granuloma formation in zebrafish embryos. Immunity. 2002; 17:693–702. [PubMed: 12479816]

De Craene B, Berx G. Regulatory networks defining EMT during cancer initiation and progression. Nat Rev Cancer. 2013; 13:97–110. [PubMed: 23344542]

Dorhoi A, Kaufmann SH. Perspectives on host adaptation in response to Mycobacterium tuberculosis: modulation of inflammation. Semin Immunol. 2014; 26:533–542. [PubMed: 25453228]

Ellett F, Pase L, Hayman JW, Andrianopoulos A, Lieschke GJ. mpeg1 promoter transgenes direct macrophage-lineage expression in zebrafish. Blood. 2011; 117:e49–e56. [PubMed: 21084707]

Ernst JD. The immunological life cycle of tuberculosis. Nat Rev Immunol. 2012; 12:581–591. [PubMed: 22790178]

Gauthier DT, Vogelbein WK, Ottinger CA. Ultrastructure of Mycobacterium marinum granuloma in striped bass Morone saxatilis. Dis Aquat Organ. 2004; 62:121–132. [PubMed: 15648839]

Hall C, Flores MV, Storm T, Crosier K, Crosier P. The zebrafish lysozyme C promoter drives myeloid-specific expression in transgenic fish. BMC Dev Biol. 2007; 7:42. [PubMed: 17477879]

Herbomel P, Thisse B, Thisse C. Ontogeny and behaviour of early macrophages in the zebrafish embryo. Development. 1999; 126:3735–3745. [PubMed: 10433904]

Marakalala MJ, Raju RM, Sharma K, Zhang YJ, Eugenin EA, Prideaux B, Daudelin IB, Chen PY, Booty MG, Kim JH, et al. Inflammatory signaling in human tuberculosis granulomas is spatially organized. Nat Med. 2016; 22:531–538. [PubMed: 27043495]

Martin CJ, Carey AF, Fortune SM. A bug's life in the granuloma. Semin Immunopathol. 2015

Medina E, North RJ. Resistance ranking of some common inbred mouse strains to Mycobacterium tuberculosis and relationship to major histocompatibility complex haplotype and Nramp1 genotype. Immunology. 1998; 93:270–274. [PubMed: 9616378]

Meijer AH, van der Sar AM, Cunha C, Lamers GE, Laplante MA, Kikuta H, Bitter W, Becker TS, Spaink HP. Identification and real-time imaging of a myc-expressing neutrophil population involved in inflammation and mycobacterial granuloma formation in zebrafish. Dev Comp Immunol. 2008; 32:36–49. [PubMed: 17553562]

Metchnikoff E. Ueber die phagocytäre Rolle der Tuberkelriesenzellen. Virchows Archiv für pathologische Anatomie und Physiologie und für klinische Medicin. 1888; 113:63–94.

Mosimann C, Kaufman CK, Li P, Pugach EK, Tamplin OJ, Zon LI. Ubiquitous transgene expression and Cre-based recombination driven by the ubiquitin promoter in zebrafish. Development. 2011; 138:169–177. [PubMed: 21138979]

Nieman MT, Kim JB, Johnson KR, Wheelock MJ. Mechanism of extracellular domain-deleted dominant negative cadherins. J Cell Sci. 1999; 112(Pt 10):1621–1632. [PubMed: 10212155]

Oehlers SH, Cronan MR, Scott NR, Thomas MI, Okuda KS, Walton EM, Beerman RW, Crosier PS, Tobin DM. Interception of host angiogenic signalling limits mycobacterial growth. Nature. 2015; 517:612–615. [PubMed: 25470057]

Parikka M, Hammaren MM, Harjula SK, Halfpenny NJ, Oksanen KE, Lahtinen MJ, Pajula ET, Iivanainen A, Pesu M, Ramet M. Mycobacterium marinum Causes a Latent Infection that Can Be Reactivated by Gamma Irradiation in Adult Zebrafish. PLoS Pathog. 2012; 8:e1002944. [PubMed: 23028333]

Philips JA, Ernst JD. Tuberculosis pathogenesis and immunity. Annu Rev Pathol. 2012; 7:353–384. [PubMed: 22054143]

Ramakrishnan L. Revisiting the role of the granuloma in tuberculosis. Nat Rev Immunol. 2012; 12:352–366. [PubMed: 22517424]

Russell DG. Who puts the tubercle in tuberculosis? Nat Rev Microbiol. 2007; 5:39–47. [PubMed: 17160001]

Schöppel, O. Untersuchungen uber Lymphdrüsen-Tuberkulose sowie über die damit verwandten und verwechselten Drüsenkrankheiten. Tübingen: Lauppsch; 1871.

Spector WG, Lykke AW. The cellular evolution of inflammatory granulomata. J Pathol Bacteriol. 1966; 92:163–167. [PubMed: 5956253]

Spector WG, Willoughby DA. The origin of mononuclear cells in chronic inflammation and tuberculin reactions in the rat. J Pathol Bacteriol. 1968; 96:389–399. [PubMed: 5698711]

Sutton JS, Weiss L. Transformation of monocytes in tissue culture into macrophages, epithelioid cells, and multinucleated giant cells. An electron microscope study. J Cell Biol. 1966; 28:303–332. [PubMed: 5914695]

Swaim LE, Connolly LE, Volkman HE, Humbert O, Born DE, Ramakrishnan L. Mycobacterium marinum infection of adult zebrafish causes caseating granulomatous tuberculosis and is moderated by adaptive immunity. Infect Immun. 2006; 74:6108–6117. [PubMed: 17057088]

Tang A, Armagai M, Granger LG, Stanley JR, Udey MC. Adhesion of epidermal Langerhans cells to keratinocytes mediated by E-cadherin. Nature. 1993; 361:82–85. PMID 8421498. [PubMed: 8421498]

Trinh LA, Hochgreb T, Graham M, Wu D, Ruf-Zamojski F, Jayasena CS, Saxena A, Hawk R, Gonzalez-Serricchio A, Dixson A, et al. A versatile gene trap to visualize and interrogate the function of the vertebrate proteome. Genes Dev. 2011; 25:2306–2320. [PubMed: 22056673]

Turner J, Gonzalez-Juarrero M, Saunders BM, Brooks JV, Marietta P, Ellis DL, Frank AA, Cooper AM, Orme IM. Immunological basis for reactivation of tuberculosis in mice. Infect Immun. 2001; 69:3264–3270. [PubMed: 11292749]

Ulrichs T, Kosmiadi GA, Trusov V, Jorg S, Pradl L, Titukhina M, Mishenko V, Gushina N, Kaufmann SH. Human tuberculous granulomas induce peripheral lymphoid follicle-like structures to orchestrate local host defence in the lung. J Pathol. 2004; 204:217–228. [PubMed: 15376257]

Van den Bossche J, Bogaert P, van Hengel J, Guerin CJ, Berx G, Movahedi K, Van den Bergh R, Pereira-Fernandes A, Geuns JM, Pircher H, et al. Alternatively activated macrophages engage in homotypic and heterotypic interactions through IL-4 and polyamine-induced E-cadherin/catenin complexes. Blood. 2009; 114:4664–4674. [PubMed: 19726720]

Van den Bossche J, Laoui D, Naessens T, Smits HH, Hokke CH, Stijlemans B, Grooten J, De Baetselier P, Van Ginderachter JA. E-cadherin expression in macrophages dampens their inflammatory responsiveness in vitro, but does not modulate M2-regulated pathologies in vivo. Sci Rep. 2015; 5:12599. [PubMed: 26226941]

van Roy F, Berx G. The cell-cell adhesion molecule E-cadherin. Cell Mol Life Sci. 2008; 65:3756–3788. [PubMed: 18726070]

Vannella KM, Barron L, Borthwick LA, Kindrachuk KN, Narasimhan PB, Hart KM, Thompson RW, White S, Cheever AW, Ramalingam TR, Wynn TA. Incomplete deletion of IL-4Ralpha by

LysM(Cre) reveals distinct subsets of M2 macrophages controlling inflammation and fibrosis in chronic schistosomiasis. PLoS Pathog. 2014; 10:e1004372. [PubMed: 25211233]

Volkman HE, Clay H, Beery D, Chang JC, Sherman DR, Ramakrishnan L. Tuberculous granuloma formation is enhanced by a mycobacterium virulence determinant. PLoS Biol. 2004; 2:e367. [PubMed: 15510227]

Volkman HE, Pozos TC, Zheng J, Davis JM, Rawls JF, Ramakrishnan L. Tuberculous granuloma induction via interaction of a bacterial secreted protein with host epithelium. Science. 2010; 327:466–469. [PubMed: 20007864]

Walton EM, Cronan MR, Beerman RW, Tobin DM. The Macrophage-Specific Promoter mfap4 Allows Live, Long-Term Analysis of Macrophage Behavior during Mycobacterial Infection in Zebrafish. PLoS One. 2015; 10:e0138949. [PubMed: 26445458]

Wanat KA, Rosenbach M, Zoiber AF, Zhang PJ, Schaffer A. E-cadherin is expressed by mono- and multinucleated histiocytes in cutaneous sarcoidal and foreign body granulomas. Am J Dermatopathol. 2014; 36:651–654. [PubMed: 23719484]

Williams GT, Williams WJ. Granulomatous inflammation--a review. J Clin Pathol. 1983; 36:723–733. [PubMed: 6345591]

Yang B, Treweek JB, Kulkarni RP, Deverman BE, Chen CK, Lubeck E, Shah S, Cai L, Gradinaru V. Single-cell phenotyping within transparent intact tissue through whole-body clearing. Cell. 2014; 158:945–958. [PubMed: 25088144]

Yang CT, Cambier CJ, Davis JM, Hall CJ, Crosier PS, Ramakrishnan L. Neutrophils exert protection in the early tuberculous granuloma by oxidative killing of mycobacteria phagocytosed from infected macrophages. Cell Host Microbe. 2012; 12:301–312. [PubMed: 22980327]

Yona S, Gordon S. From the Reticuloendothelial to Mononuclear Phagocyte System - The Unaccounted Years. Front Immunol. 2015; 6:328. [PubMed: 26191061]

Zakrzewska A, Cui C, Stockhammer OW, Benard EL, Spaink HP, Meijer AH. Macrophage-specific gene functions in Spi1-directed innate immunity. Blood. 2010; 116:e1–e11. [PubMed: 20424185]

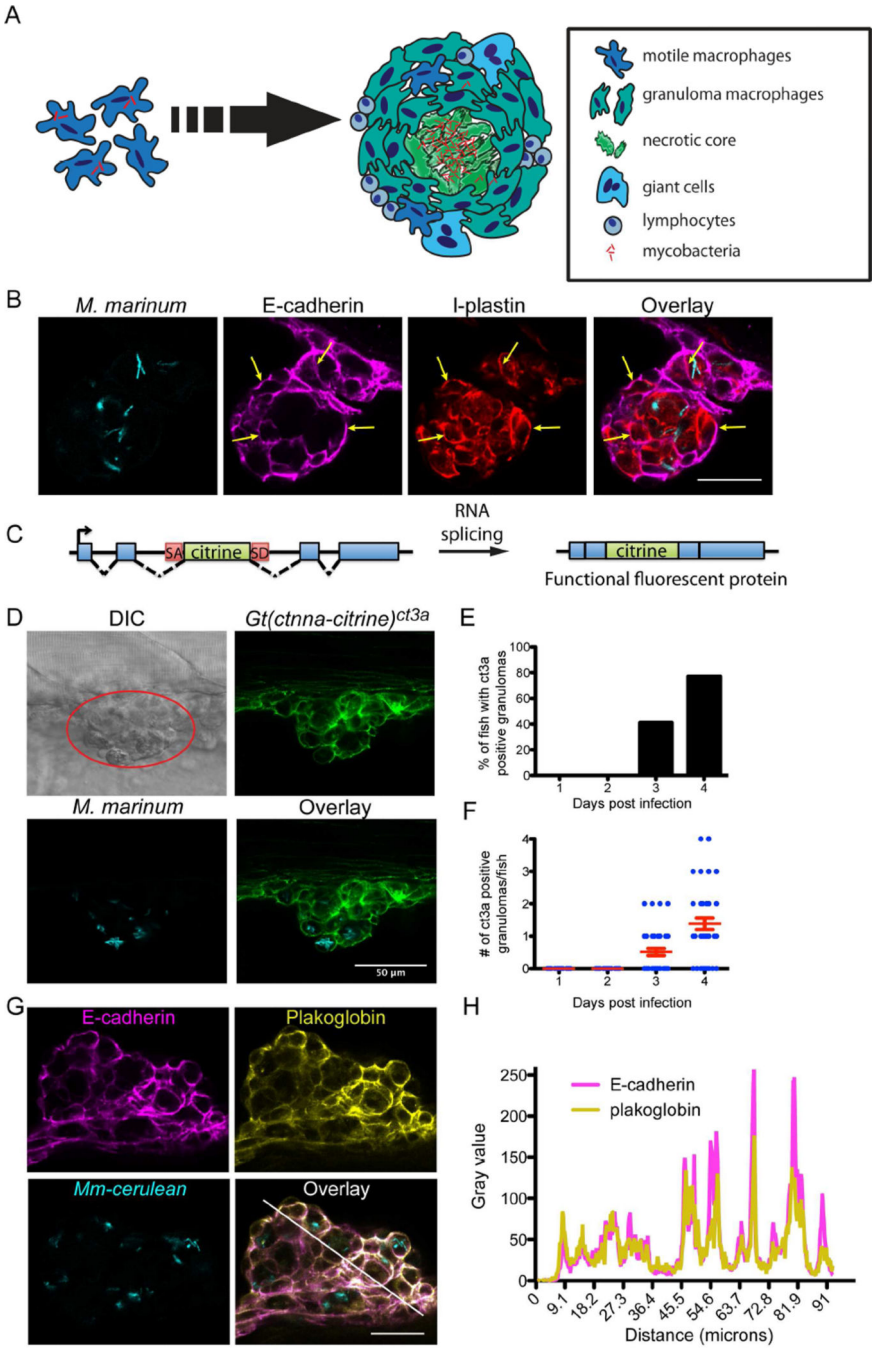

Figure 1. Mycobacterial Granulomas in Larvae Induce Expression of Epithelial Markers

(A) Cartoon of granuloma formation depicting macrophage aggregation and morphological rearrangement to an interdigitated, flattened epithelial appearance. (B) *M. marinum* (cyan) granulomas stained for E-cadherin (magenta) and l-plastin (red) at 4 dpi in larva infected with 250 fluorescent *M. marinum*. Scale bar – 25 μm. (C) Schematic of gene trap approach used in generating the *Gt(ctnna-citrine)*^{ct3a} and *Gt(jup-citrine)*^{ct520a}zebrafish lines: an exogenous citrine ORF flanked with a splice donor site (SD) and splice acceptor (SA) is introduced into the endogenous *ctnna* and *jup* genes. (D) Granulomas were identified by

DIC imaging (red circle). Fluorescent imaging demonstrating localization of *Gt(ctnna-citrine)*^{ct3a} fusion protein (green) at adherens junctions formed in *M. marinum* (cyan) larval granulomas at 4 dpi. Scale bar – 50 μm. (E and F) Quantitation of *Gt(ctnna-citrine)*^{ct3a} positive granulomas from 1–4 dpi in larval zebrafish infected with 150–250 fluorescent bacteria (FB)/fish *M. marinum* n = 39, representative of 3 independent experiments. (E) Percentage of fish with at least one *Gt(ctnna-citrine)*^{ct3a} positive granuloma by day. (F) Number of *Gt(ctnna-citrine)*^{ct3a} positive granulomas per fish. Each dot represents one fish. Bars represent mean ± SEM. (G) Fluorescent images of a 4 dpi larval granuloma showing E-cadherin staining (magenta) colocalized with plakoglobin (yellow) in a granuloma in *M. marinum* (cyan)-infected zebrafish. Fish were infected with 150–250 FB/fish. Scale bar – 25 μm. Images representative of results from 12 animals. (H) Plakoglobin and E-cadherin fluorescence intensity as a function of distance was measured along the white line in (G), demonstrating colocalization of E-cadherin fluorescence with plakoglobin. See also Figure S1.

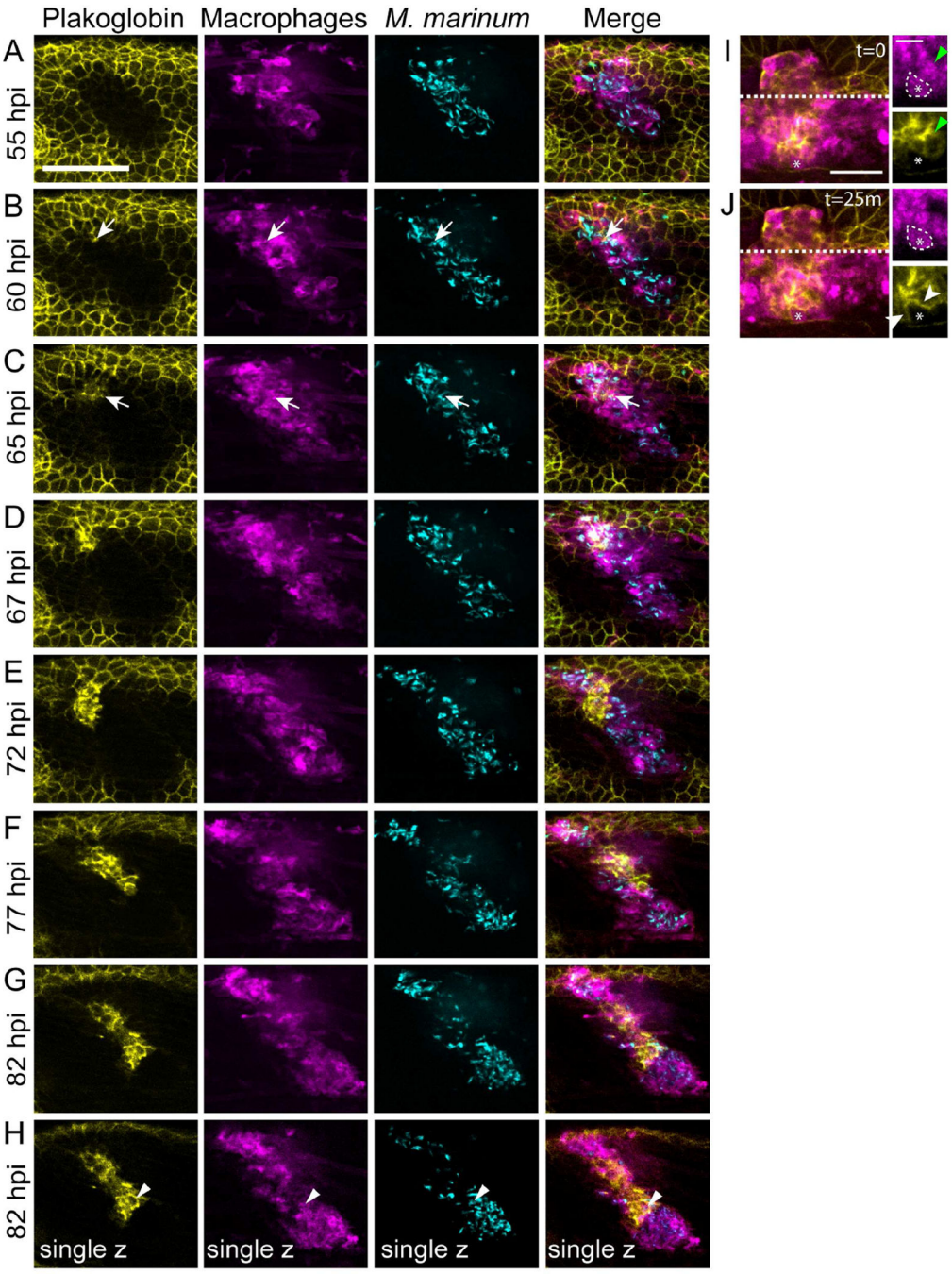

Figure 2. Live Imaging of Adherens Junction Formation within Macrophages of the Developing Granuloma

Tg(mfap4:tomato-caax); Gt(jup-citrine)^{ct520a} animals were infected with 150–250 FB/fish and imaged from 48 hours post infection (hpi) to 96 hpi to visualize adherens junction formation during granuloma formation. (A–G) The image in each panel is a maximum projection of a 28 μm z-stack. Arrows indicate the site of initial adherens junction formation within the granuloma. Scale bar – 100 μm. (H) single z-plane image from 82 hpi timepoint demonstrating plakoglobin adherens junction formation within granuloma macrophages. Arrowheads indicate a plakoglobin-positive infected macrophage in single plane image.

Gamma adjustments were applied uniformly across all images to facilitate display. Note – the initial plakoglobin signal surrounding the granuloma is the larval skin within the imaging planes. (I) and (J) Images of a granuloma in another *Tg(mfap4:tomato-caax); Gt(jup-citrine)*^{ct520a} animal demonstrating formation of adherens junctions (plakoglobin, yellow) between adjacent macrophages (magenta). (I) A plakoglobin-negative approaching macrophage (white dotted line, asterisk) contacts a plakoglobin-positive macrophage (green arrowheads). (J) 25 minutes later, the macrophage relocalizes plakoglobin to the cell surface (white arrowheads). Scale bar – 100 μm in main image, 50 μm in inset. See also Movies S1 and S2.

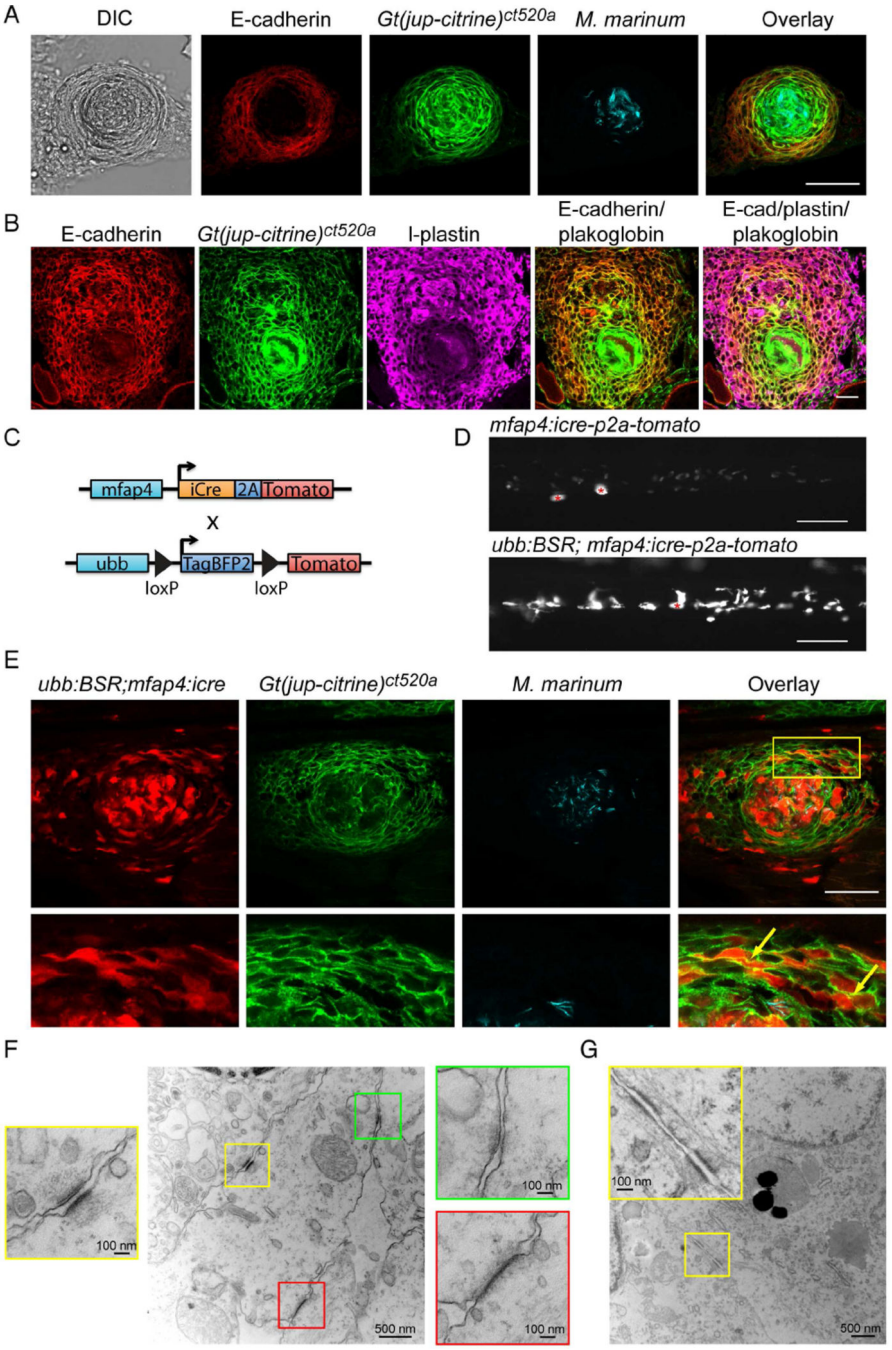

Figure 3. Granuloma Epithelialization Occurs within Macrophages and Involves Multiple Adhesive Pathways

(A) E-cadherin was detected by immunofluorescence (red) and colocalized with endogenous *Gt(jup-citrine)*^{ct520a} (green) in granulomas in 2 wpi *M. marinum* (cyan) infected animals. Scale bar – 50 μm. (B) E-cadherin staining (red) and plakoglobin fluorescence (green) within cell populations that are positive for the pan-leukocyte marker l-plastin (magenta) in granulomas from 2 wpi animals. Scale bar – 25 μm. (C) Diagram of lineage tracing approach used to label macrophages. (D) Images of tdTomato expression in animals expressing either macrophage-specific Cre alone (Tg(mfap4:icre-p2a-tomato)) or double transgenic animals in

which macrophage specific Cre rearranges the blue-to-red lineage tracing cassette (Tg(ubb:BSR; mfap4:icre)), resulting in robust red fluorescence from the reporter cassette. Asterisks mark autofluorescent melanocytes. Scale bar – 100 μm. (E) A necrotic granuloma in a 2 wpi *Tg(mfap4:icre; ubb:BSR); Gt(jup-citrine)*^{ct520a} animal infected with 400 FB of cerulean-tagged mycobacteria. Images show macrophages (red) localizing to plakoglobin positive adherens junctions (green); infecting mycobacteria are visualized in cyan. Yellow box indicates magnified areas shown in the row below. Images are representative of granulomas from 12 animals. Scale bar – 50 μm. (F) Electron microscopy images of desmosomes (yellow box), adherens junctions (green box) and tight junctions (red box) in granuloma macrophages in *M. marinum* infected 2 wpi *Tg(mfap4:icre; ubb:BSR)* zebrafish. (G) Image of desmosomes in 2 wpi *Tg(mfap4:icre; ubb:BSR)* zebrafish. Note in inset the filament network associated with desmosomes. See also Figure S2 and S3.

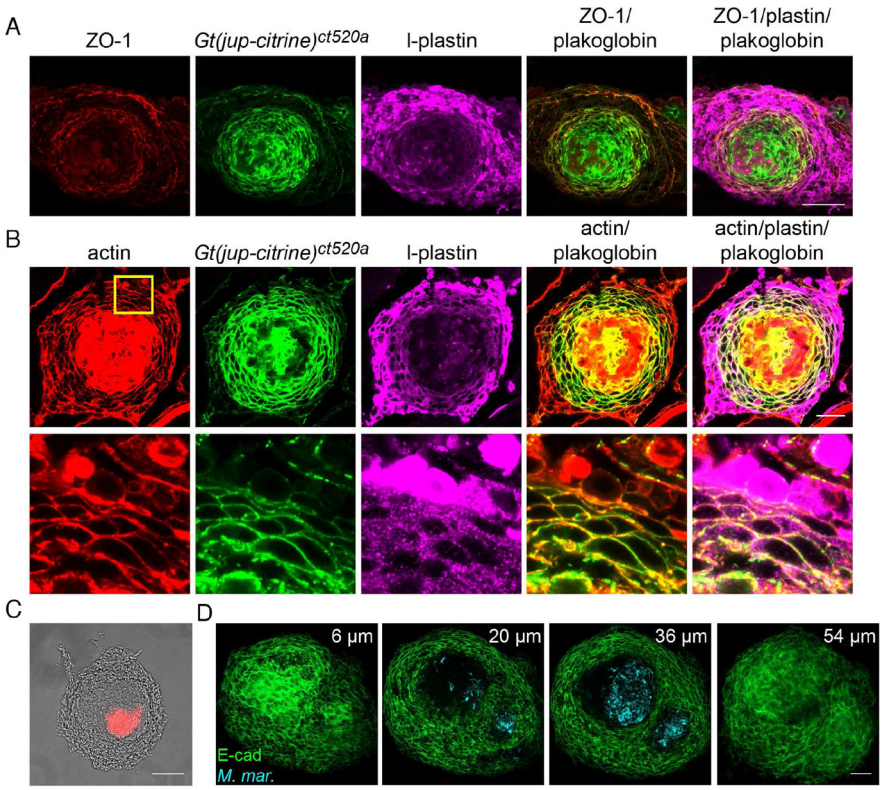

F

KEGG pathways altered in granulomas	p value	q value
Cytokine-cytokine receptor interaction	1.41E-13	1.97E-11
Focal adhesion	6.83E-07	4.78E-05
Cell adhesion molecules (CAMs)	1.98E-06	7.8E-05
Tight junction	2.17E-06	7.5E-05
ECM-receptor interaction	5.26E-06	0.000147
Steroid biosynthesis	3.14E-05	0.000734
Arachidonic acid metabolism	5.45E-05	0.00109
Glycine, serine and threonine metabolism	0.000115	0.001738
Histidine metabolism	0.000118	0.001738
Lysosome	0.000124	0.001738
Arginine and proline metabolism	0.000155	0.001835
Drug metabolism - cytochrome P450	0.000157	0.001835
Metabolism of xenobiotics by cytochrome P450	0.000236	0.002537
Other glycan degradation	0.000378	0.003781
Retinol metabolism	0.000473	0.004318
Regulation of actin cytoskeleton	0.000493	0.004318
Phagosome	0.000564	0.004644
Intestinal immune network for IgA production	0.000619	0.004816
Glutathione metabolism	0.000855	0.0063
Phenylalanine metabolism	0.001356	0.009491
Adherens junction	0.002938	0.019585
PPAR signaling pathway	0.005581	0.035514

G

Gene Short Name	Gene Long Name	Mean FPKM Macrophages	Mean FPKM Granulomas	Log2 differential expression	Adjusted p Value
	Adherens Junctions				
cdh1	cadherin 1, epithelial	15.968	206.686	3.694	1.03E-06
ctnna1	catenin, alpha 1	21.033	55.344	1.396	0.015
ctnnb2	catenin, beta 2	16.605	57.611	1.795	0.00064
ctnnd1	catenin, delta 1	24.670	123.857	2.328	7.70E-05
jupa	junction plakoglobin a	51.402	543.004	3.401	3.28E-45
	Tight Junctions				
tjp1a	tight junction protein 1a (ZO-1)	1.492	19.907	3.738	1.03E-24
tjp2b	tight junction protein 2b (ZO-2)	18.873	176.677	3.227	2.00E-10
cldn12	claudin 12	16.011	51.142	1.675	1.55E-05
cldne	claudin e	0.076	19.242	7.975	5.31E-17
oclna	occludin a	23.021	122.137	2.407	0.0071
	Desmosomes				
dspa	desmoplakin a	9.176	167.442	4.190	3.16E-16
dsg2.1	Desmoglein 2, tandem duplicate 1	1.884	32.648	4.115	9.03E-05
dsc2l	desmocollin 2 like	4.340	96.556	4.476	1.09E-09
pkp1b	plakophilin 1b	2.459	164.476	6.064	1.78E-14
pkp3a	plakophilin 3	2.359	69.494	4.881	3.31E-10
	Cell Polarity				
pard3	partitioning defective 3 homolog	0.601	3.301	2.457	0.0014
parc6a	partitioning defective 6 homolog alpha	0.428	12.176	4.829	2.92E-13
prkcz	protein kinase C, zeta	0.310	2.269	2.871	1.52E-05
crb3a	Crumbs homolog 3a	0.890	21.567	4.599	4.21E-15
scrib	scribbled homolog	5.737	3.915	-0.551	0.42
dlg1	discs large homolog 1	1.640	25.395	3.953	4.60E-05
llg1	lethal giant larvae homolog 1	2.218	30.589	3.786	3.59E-06
	Macrophage/Leukocyte Markers				
ITGAL	Integrin subunit alpha L	120.351	114.812	-0.068	0.96
itgam	integrin, alpha M	6.135	2.978	-1.043	0.13
itgb2	integrin, beta 2	108.438	43.059	-1.332	0.00042
lcp1	Lymphocyte cytosolic protein 1 (L-plastin)	594.079	94.680	-2.650	2.27E-09
CD68	CD68 molecule	598.903	117.852	-2.345	6.96E-08
csf1ra	colony stimulating factor 1 receptor, a	33.422	6.951	-2.266	0.00053
mpeg1.1	Macrophage expressed 1 (MPEG1)	424.069	15.631	-4.762	2.79E-18
mfap4	microfibrillar-associated protein 4	933.889	43.785	-4.414	2.81E-17
	Cytokines				
tnfa	tumor necrosis factor a	154.239	1730.512	3.488	0.0015
ifng1-2	interferon, gamma 1-2	0.769	8.065	3.390	0.035

Figure 4. Granuloma Formation is Accompanied by Diverse Changes in Macrophage Cytoskeleton and Gene Expression

(A) ZO-1 immunofluorescence (red) localized within the plakoglobin (green) positive region surrounding the granuloma necrotic core in l-plastin positive cells (magenta) in 2 wpi *M. marinum* infected animals at an initial dose of 400 FB. Results representative of granulomas in 4 animals. Scale bar – 50 µm. (B) Actin (red) and plakoglobin (*Gt(jup-citrine)*^{ct520a}, green) localization within the l-plastin (magenta) positive cells of the granuloma. Cortical reorganization of actin occurs within l-plastin positive granuloma cells that have cell-surface localized plakoglobin. Yellow box indicates area magnified in bottom panel. Representative

of results from 4 animals. (C) Phase contrast image of a granuloma dissected from a 2 wpi zebrafish infected with 400 FB of *M. marinum*. *M. marinum* fluorescence overlaid in red on the phase contrast image. Scale bar – 100 μm. (D) Dissected, CLARITY-cleared granuloma stained for E-cadherin (green) from a 2 wpi *M. marinum* (cyan) infected animal. (E) Hierarchical clustering of expression data from dissected granulomas and kidney macrophages from infected animals. Darker colors on the heat map indicate samples with more closely related transcriptomes. (F) Most differentially regulated pathways in granulomas relative to kidney macrophages from infected animals. (G) Expression changes between kidney macrophages and granulomas in selected adhesion, polarity and immune marker genes. Mean transcript expression levels are calculated as fragments mapped per kilobase of exon per million fragments mapped (FPKM). Differential expression values are calculated as Log_2(granuloma/macrophages). More complete tables of pathway components available in Table S1 and within the complete dataset in Table S2. See also Figures S3 and S4.

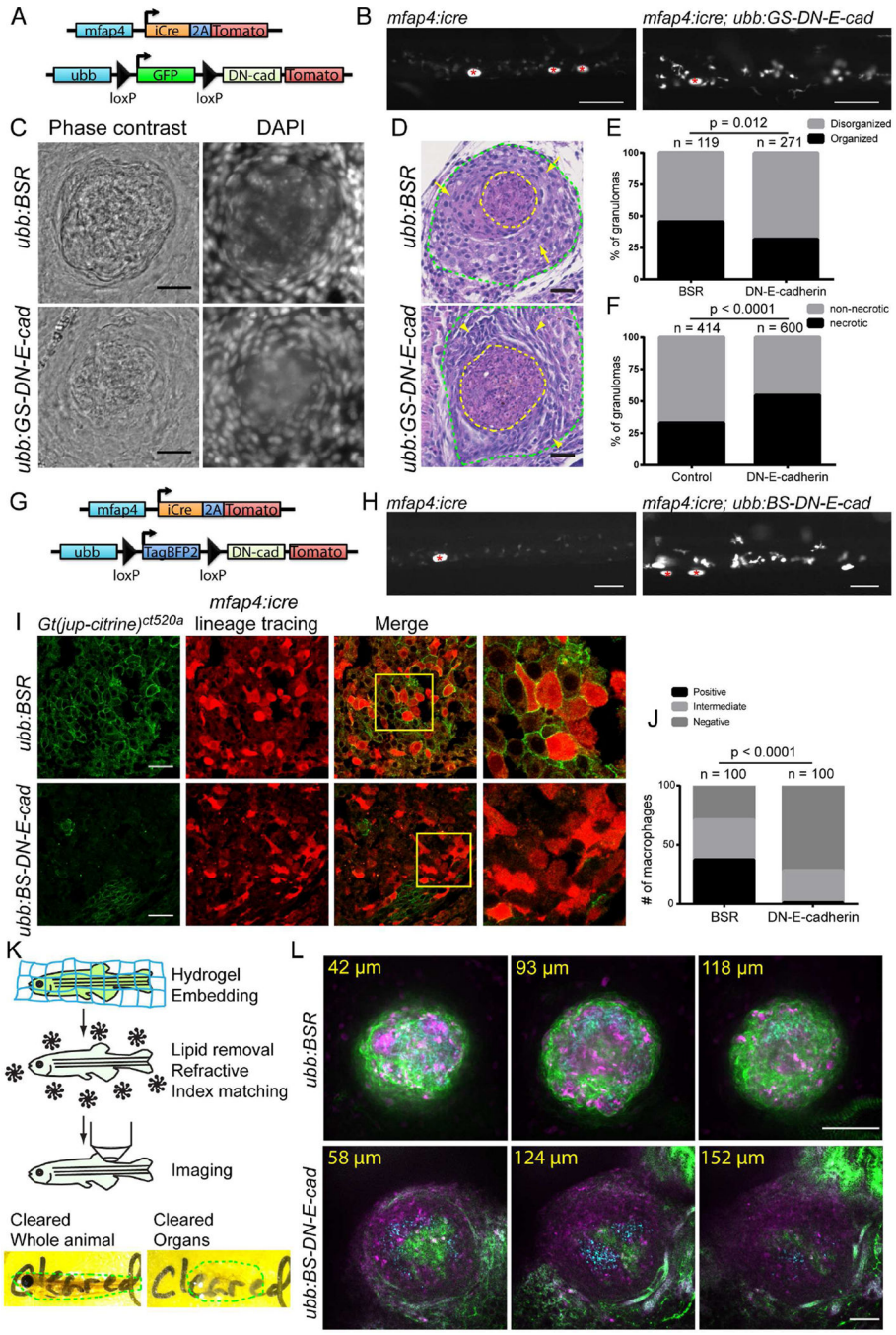

Figure 5. Cadherin-dependent Adherens Junctions Promote Granuloma Organization

(A) Schematic of lineage tracing approach used to drive DN-E-cadherin within macrophages. (B) Images of tomato expression in *Tg(mfap4:icre)* and *Tg(mfap4:icre; ubb:GS-DN-e-cadherin)* animals showing increased tomato expression in *Tg(mfap4:icre; ubb:GS-DN-e-cadherin)* animals relative to *Tg(mfap4:icre)* animals, indicative of rearrangement of the lineage tracing DN-E-cadherin cassette. Asterisks mark autofluorescent melanophores. Scale bar – 100 µm. (C) Images of 2 wpi *M. marinum* granulomas in *Tg(mfap4:icre; ubb:BSR); Gt(jup-citrine)*^{ct520a} and *Tg(mfap4:icre; ubb:GS-*

DN-e-cadherin) fish showing the morphology of granulomas by phase contrast and DAPI staining of granuloma nuclei. Animals were infected with 400 FB/fish *M. marinum*. Scale bar – 25 μm. (D) H&E stained sections from *Tg(mfap4:icre; ubb:BSR); Gt(jup-citrine)*^{ct520a} and *Tg(mfap4:icre; ubb:GS-DN-e-cadherin)* demonstrating morphological alterations in DN-E-cadherin expressing animals. Sections from 2 wpi animals infected with 400 FB/fish *M. marinum*. Yellow dotted lines denote necrotic cores of individual granulomas. Green lines indicate regions of macrophages surrounding the necrotic core. Arrows indicate cells with classical epithelioid morphology within *Tg(mfap4:icre; ubb:BSR)* animals. Arrowheads mark groups of epithelioid macrophages with spindle morphology. Scale bars – 25 μM. (E–F) Quantitation of necrotic granulomas in pooled *Tg(mfap4:icre; ubb:BSR); Gt(jup-citrine)*^{ct520a} and DN-E-cadherin expressing animals (*mfap4:icre; ubb:GS-DN-e-cadherin* and *mfap4:icre*; *ubb:BS-DN-e-cadherin*) from 3 experiments. (E) Organization of cells surrounding the necrotic core, visualized by brightfield as outlined in Figure S4D. P value determined by Fisher's exact test and (F) The percentage of necrotic granulomas in each fish. Populations compared by Fisher's exact test. (G) Schematic of lineage tracing approach used to drive rearrangement of the *Tg(ubb:BS-DN-e-cadherin)* construct leading to DN-E-cadherin expression in macrophages. (H) Images of *Tg(mfap4:icre)* and *Tg(mfap4:icre*; *ubb:BS-DN-e-cadherin)* animals demonstrating expression of DN-E-cadherin in macrophages through increased tomato fluorescence from the downstream 2A tomato cassette. Asterisks mark autofluorescent melanocytes. Scale bar – 100 μm. (I) Images of macrophage localization (red, *mfap4:icre* lineage tracing) and plakoglobin positive adherens junctions (green, *Gt(jup-citrine)*^{ct520a}) of granulomas formed in control *Tg(mfap4:icre; ubb:BSR); Gt(jup-citrine)*^{ct520a} and *Tg(mfap4:icre*; *ubb:BS-DN-e-cadherin); Gt(jup-citrine)*^{ct520a}) animals. Boxes indicate regions of the merged image magnified in the images to the right. Scale bar – 25 μm. (J) Quantitation of plakoglobin expression within macrophages in non-necrotic granulomas from either control *Tg(mfap4:icre; ubb:BSR); Gt(jup-citrine)*^{ct520a} or DN-E-cadherin expressing macrophages from *Tg(mfap4:icre*; *ubb:BS-DN-e-cadherin); Gt(jup-citrine)*^{ct520a} animals. Macrophages were scored for plakoglobin positivity as outlined in experimental procedures. Quantitation from 5 granulomas in 2 animals each. Populations were compared by Chi square test. (K) Top - Cartoon of the steps of CLARITY-mediated tissue clearing in zebrafish. Bottom - images of cleared intact zebrafish and zebrafish organs. Dotted lines indicate the extent of the individual tissues. (L) Imaging of intact, CLARITY cleared granulomas in *Tg(mfap4:icre; ubb:BSR); Gt(jup-citrine)*^{ct520a} and *Tg(mfap4:icre*; *ubb:BS-DN-e-cadherin); Gt(jup-citrine)*^{ct520a} animals demonstrating loss of adherens junctions and organization in DN-E-cadherin animals. Green – plakoglobin, magenta – macrophages, *M. marinum* – cyan. Micron distances indicate the depth of each individual image relative to the top of the granuloma. Scale bar – 100 μm. For CLARITY images, gamma adjustment was performed uniformly for display. See also Figures S4 and S5 and Movies S3–S5.

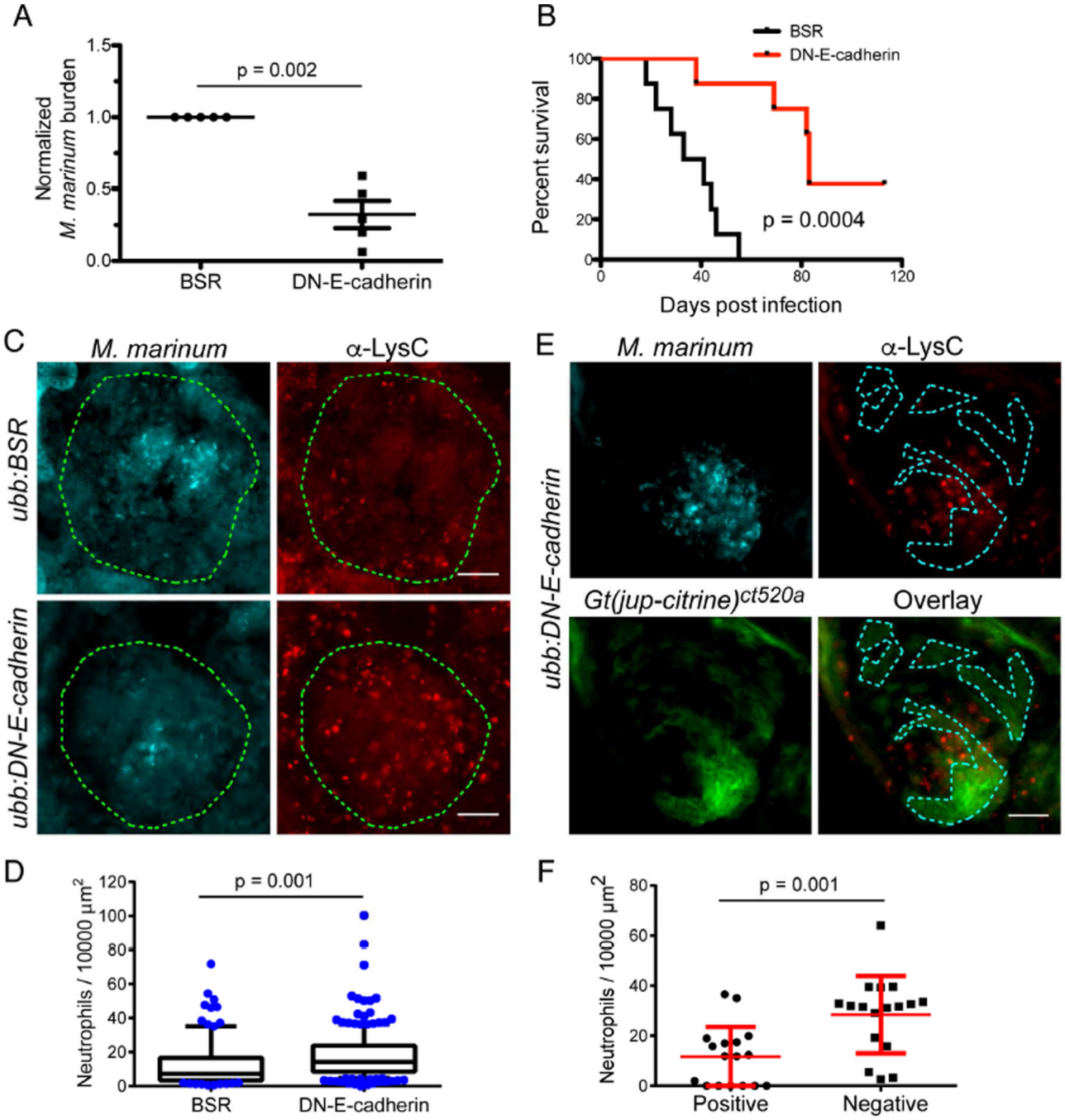

Figure 6. Loss of Granuloma Adherens Junctions Reduces Bacterial Burden and Enhances Survival of Infected Animals

(A) Bacterial burden in *Tg(mfap4:icre; ubb:BSR)* and *Tg(mfap4:icre; ubb:GS-DN-e-cadherin)* animals was determined by CFU counts from whole animals at 2 wpi. Each point represents the mean of a single experiment with 5–8 surviving fish of each genotype in each experiment. Due to CFU variability between experiments, each experiment is presented normalized to control animals. Animals were infected with either 50 FB/fish or 400 FB/fish. Bars represent mean ± SEM. (B) Survival curves of *Tg(mfap4:icre; ubb:BSR)* and *Tg(mfap4:icre; ubb:GS-DN-e-cadherin)* animals infected with 400 FB/fish and followed

longitudinally. Animals were monitored daily and moribund animals were euthanized. Statistical significance was determined by log-rank test. n = 8 for both *Tg(mfap4:icre; ubb:BSR)* and *Tg(mfap4:icre; ubb:GS-DN-e-cadherin)* groups. Experiments are representative of 3 independent experiments, additional experiments are displayed as Figures S5C and S5D. (C) *M. marinum* fluorescence (cyan) and neutrophil localization visualized by anti-LysC immunostaining (red) in *Tg(mfap4:icre; ubb:BSR); Gt(jup-citrine)*^{ct520a} and *Tg(mfap4:icre*; *ubb:BS-DN-e-cadherin); Gt(jup-citrine)*^{ct520a} animals demonstrating increased neutrophil recruitment to granulomas in DN-E-cadherin expressing animals. The extent of each granuloma is indicated by the dotted lines. Scale bar – 25 μm. (D) Quantitation of neutrophil numbers (normalized to area) in *Tg(mfap4:icre; ubb:BSR); Gt(jup-citrine)*^{ct520a} and *Tg(mfap4:icre*; *ubb:BS-DN-e-cadherin); Gt(jup-citrine)*^{ct520a} animals. Box indicates 25% and 75% percentile, and whiskers 10%-90% percentile. Outliers indicated as individual points. For control granulomas, n = 107; for DN-E-cadherin granulomas, n = 209. Results pooled over 6 animals in controls and 9 animals in DN-E-cadherin. (E) Mycobacteria (cyan), neutrophils (red, α-LysC) and plakoglobin (green, *Gt(jup-citrine)*^{ct520a}) in *Tg(mfap4:icre*; *ubb:BS-DN-e-cadherin); Gt(jup-citrine)*^{ct520a} animals demonstrating preferential recruitment of neutrophils to regions of the granuloma devoid of plakoglobin-positive adherens junctions. Dotted line denotes regions of plakoglobin-positive adherens junction formation. Scale bar – 25 μm. (F) Quantitation of area-normalized neutrophil counts in plakoglobin positive and plakoglobin negative regions of *Tg(mfap4:icre*; *ubb:BS-DN-e-cadherin); Gt(jup-citrine)*^{ct520a} animals. Only granulomas in which distinct plakoglobin positive and negative regions could be identified were analyzed. Data from 17 granulomas from 3 independent animals. See also Figures S5 and S6.

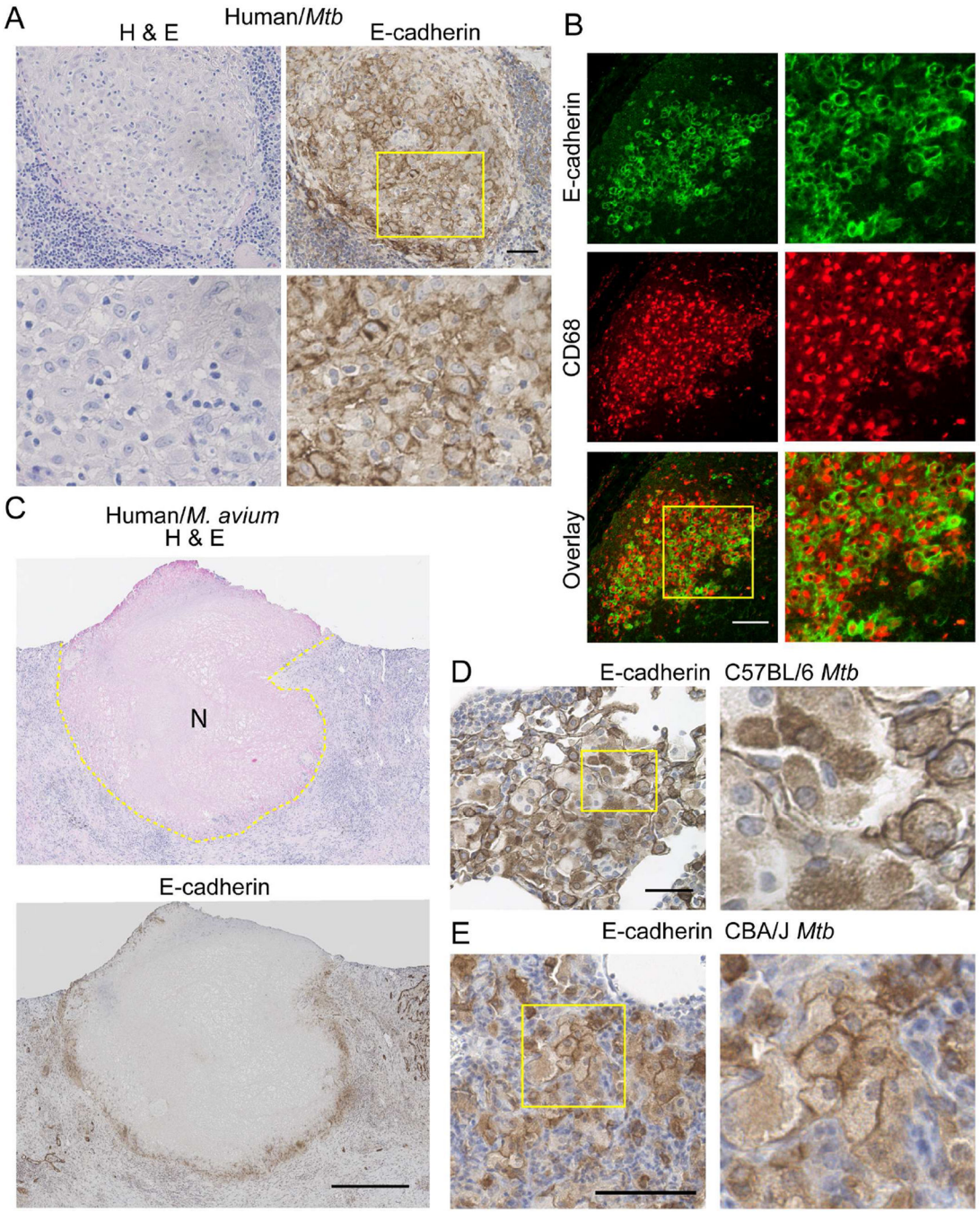

Figure 7. E-cadherin Is Expressed in Granuloma Macrophages in Human *Mtb* Patients and Mouse Models

(A) Left – H&E staining of a human lymph node granuloma from a patient with disseminated *Mtb* infection. Right – Representative immunohistochemical image of E-cadherin (brown precipitate) in human *Mtb* lymph node sample showing junctional localization of E-cadherin within epithelioid macrophages. Nuclei are counterstained with hematoxylin. Yellow box indicates the area magnified in the bottom panels. Scale bar – 50 μm. (B) Representative double immunofluorescence of a human *Mtb* lymph node granuloma demonstrating expression of E-cadherin (green) within CD68 positive macrophages (red).

Scale bar – 100 μm. (C) Top – H&E staining of a necrotic *M. avium* granuloma in the lung. Central necrotic region is visualized as eosinophilic focus devoid of hematoxylin positive nuclei marked with N. The extent of the necrotic core is outlined in the dotted lines. Bottom – Representative immunohistochemical staining of E-cadherin within an *M. avium* lung granuloma. Extensive E-cadherin staining is seen in the palisading macrophages immediately surrounding the necrotic core. Scale bar – 500 μm. (A–C) Images representative of 9 granulomas from 8 independent patients with mycobacterial granulomas, all of which were positive for E-cadherin staining. (D) Diffuse E-cadherin (brown precipitate) is seen throughout granuloma macrophages in 8 wpi H37Rv *Mtb* granulomas in C57BL/6 mouse lung. Nuclei are counterstained with hematoxylin. Scale bar – 50 μm. (E) E-cadherin (Brown) localizes to cell-cell junctions between granuloma macrophages in 135 dpi granulomas in CBA/J mice infected with *Mtb* Erdman. See also Figure S7.